ChemPubSoc Europe

DOI: 10.1002/open.201500034

Open Access ChemistryOPEN Full Papers

Picking Out Logic Operations in a Naphthalene β-Diketone Derivative by Using Molecular Encapsulation, Controlled Protonation, and DNA Binding

Sameena Yousuf,[a] Ritty Alex,[a] Paulraj Mosae Selvakumar,*[a] Israel V. M. V. Enoch,*[a] Palani Sivagnana Subramanian,[b] and Yu Sun[c]

On–off switching and molecular logic in fluorescent molecules are associated with what chemical inputs can do to the structure and dynamics of these molecules. Herein, we report the structure of a naphthalene derivative, the fashion of its binding to β-cyclodextrin and DNA, and the operation of logic possible using protons, cyclodextrin, and DNA as chemical inputs. The compound crystallizes out in a keto-amine form, with intramolecular N–H···O bonding. It shows stepwise formation of 1:1 and 1:2 inclusion complexes with β-cyclodextrin. The aminopentenone substituents are encapsulated by β-cyclodextrin, leaving out the naphthalene rings free. The binding constant of the β-cyclodextrin complex is 512 M^{-1}. The pK_a value of the guest molecule is not greatly affected by the complexation. Dual input logic operations, based on various chemical inputs, lead to the possibility of several molecular logic gates, namely NOR, XOR, NAND, and Buffer. Such chemical inputs on the naphthalene derivative are examples of how variable signal outputs based on binding can be derived, which, in turn, are dependent on the size and shape of the molecule.

Introduction

Since the presentation of the first information-processing molecules,[1] examination of chemical compounds in light of their Boolean logic functions and their possible applications has shown remarkable progress.[2,3] It is likely that such logic devices will find applications in medicine,[4] biotechnology,[5] and physiology.[6] These logic devices have shown substantial and intriguing results and have been envisaged to have some notable applications: 1) A reliable detection of pathophysiological conditions is possible with molecular logic systems;[7] 2) secure, economic, and simple methods can be developed for designing complex DNA-based logic devices;[8] 3) the molecular Boolean logic language can function as a medical diagnostic protocol;[9] 4) encapsulated drugs can be trigger-released through logic response;[10] 5) dually controlled photodynamic therapy is practicable using the AND logic gate as the template; 6) the DNA-binding of drugs can be controlled using external or internal stimuli based on a molecular switching principle;[11] and 7) molecular logic gates can be used in fluorescent papers and applied to cryptography.[12]

In one example, an AND logic gate was used as the template in photodynamic therapy involving a boron-dipyrromethene (BODIPY) derivative, and H^+ and Na^+ served as the inputs.[13] H^+ is a sensory and internal input, and could be important because the pH of cancer cells is lower than for healthy cells.[14,15] By measuring the drop in pH value, a biochemical filtering process can be realized in a signal transduction logic system.[16] The absorption and fluorescence characteristics of luminescent molecules in solution are altered by the change of pH,[17,18] and encapsulation of acidic small molecules by cyclodextrin can alter their pK_a values.[19] Cyclodextrins (β-CD) are tapered-cone-like cyclic oligosachcharides with a hydrophobic cavity capable of accommodating appropriately sized organic guest molecules.[20] The guest molecule's fluorescence is generally switched on by the host–guest complex formation with cyclodextrin. Hence, studies on chemical sensing, molecular logic design, and small object recognition could take advantage of cyclodextrin as a host structure.[21] Molecules having multiple light-emissive electronic excited states are pertinent switching structures,[22] and naphthalene derivatives are examples.[23] Their acidities are quite varied, and in their cyclodextrin inclusion complexes, they can show varying acidity responses depending on the part of the derivative molecule en-

[a] S. Yousuf, R. Alex, P. M. Selvakumar, Dr. I. V. M. V. Enoch
Department of Chemistry, Karunya University
Coimbatore 641114, Tamil Nadu (India)
E-mail: drisraelenoch@gmail.com
mosae@karunya.edu

[b] Dr. P. S. Subramanian
Department of Inorganic Materials and Catalysis, Central Salt and Marine Chemicals Research Institute, Gujarat 364021 (India)

[c] Dr. Y. Sun
Faculty of Chemistry, Kaiserslautern University of Technology
67663 Kaiserslautern (Germany)

Supporting information for this article is available on the WWW under http://dx.doi.org/10.1002/open.201500034. The absorption and fluorescence spectra showing the effect of pH on H2acacnn and the plots of the binding titration between H2acacnn and DNA are given in the Supporting Information.

gulfed by the cyclodextrin cavity.[24] Hence, it is of paramount importance to study the detailed mode of binding of guest molecules to cyclodextrin.

Besides being sensitive to protonation and cyclodextrin complexation, the fluorescence signals of β-diketone naphthalene derivatives can be switched on and off by the addition of DNA, as these compounds are switchable DNA intercalators.[25] Either DNA itself[26] or the DNA-binding of small molecules could function as biologically relevant logic gates, with possible applications in anticancer drug action.[27] Despite the importance of cyclodextrin and DNA as molecules having size- and shape-specificity in binding events and the on/off switch response of fluorescent molecules upon binding, the combined inputs of these molecules has not yet been reported. Herein, we report the synthesis, mode of binding to cyclodextrin and DNA, and molecular logic operations of (*Z*)-5-(5-((*Z*)-4-oxopent-2-en-2-ylamino)naphthalen-1-ylamino)pent-3-en-2-one (abbreviated as H_2acacnn).

Results and Discussion

Crystal and molecular structure of H_2acacnn

H_2acacnn crystallizes in the monoclinic space group *P*21/*n*, and the crystallographic data, selected H-bond lengths, and bond angles are given in Table 1. The Oak Ridge Thermal Ellipsoid Plot (ORTEP) drawing of the molecule is shown in Figure 1.

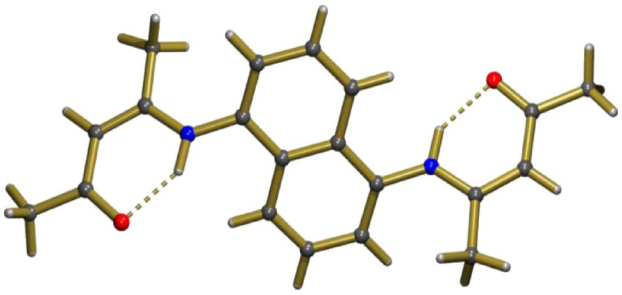

Figure 1. ORTEP diagram of the ligand with 50% probability for the thermal ellipsoid.

The single crystal X ray structure of H_2acacnnconfirms that the keto amine form is available in the solid state. The aliphatic part of the compound shows an intramolecular N–H···O interaction within the unit (Figure 1). The hydrogen atom H^1 from the amine nitrogen N^1 is involved in the intramolecular N–H…O interaction with carbonyl group which is in the same plane. In order to make an effective N–H···O interaction, the terminal aliphatic moieties are tilted 43.3° with the NH-substituted naphthyl ring within the hydrogen-bonding distance as depicted in Figure 1. The amino hydrogen NH^1 acts as a donor and is involved in the N–H···O bonding, with the O^1 of the keto group acting as an acceptor. The hydrogen-bonding distances are as follows: N^1–H^1···O^1: N^1···O^1 = 2.634 Å, H^1···O^1 = 1.843 Å, and N^1–CH^1···O^1 = 144.3°. The crystal structure confirms that the *Z*-configuration of the olefinic bond is stabilized by intramolecular N–H···O interactions between the amine and keto groups. The possible tautomers, ionic and hydrogen-bonding interactions, and *E*, *Z* isomers are shown in Scheme 1

Table 1. Crystal data and structure refinement for H_2acacnn.

Crystal Data		
CCDC Number[a]	CCDC 927799	
Empirical formula	$C_{20}H_{22}N_2O_2$	
Formula weight	322.40	
Crystal color and habit	colorless prism	
Crystal size (mm)	0.24×0.12×0.07	
Temperature (K)	150(2)	
Wavelength (Å)	1.54184	
Crystal system	monoclinic	
Space group	$P2_1/n$	
Unit cell dimensions	a = 8.0857(1) Å	α = 90°
	b = 9.1244(1) Å	β = 108.278(2)°
	c = 12.0067(2) Å	γ = 90°
Volume (Å^3)	841.13(2)	
Z	2	
Calculated density (g cm^{-3})	1.273	
Absorption coefficient (mm^{-1})	0.658	
F(000)	344	
θ-range for data collection (°)	5.85/62.65	
Index ranges	$-9 \le h \le 9$, $-10 \le k \le 10$, $-13 \le l \le 13$	
Reflections collected	6946	
Independent reflections	1336 (R_{int} = 0.0267)	
Completeness to θ = 62.65°	99.2%	
Absorption correction	Semiempirical from equivalents (Multi-scan)	
Max. and min. transmission	1.00000 and 0.91065	
Refinement method	Full-matrix least-squares on F^2	
Data/restraints/parameters	1336/1/115	
Goodness-of-fit on F^2	1.144	
Final R indices [$I > 2\sigma(I)$]	R_1 = 0.0341, wR_2 = 0.1004	
R indices (all data)	R_1 = 0.0399, wR_2 = 0.1033	
Extinction coefficent	0.011(2)	
Largest diff. Peak and hole (e·Å^{-3})	0.193/−0.190	

$$R_1 = \frac{\sum ||F_o| - |F_c||}{\sum |F_o|},\ wR_2 = \sqrt{\frac{\sum [w(F_o^2 - F_c^2)^2]}{\sum [w(F_o^2)^2]}},\ GooF = \sqrt{\frac{\sum [w(F_o^2 - F_c^2)]}{(n-p)}}$$

n = number of reflections; p = number of parameters

[a] CCDC 927799 contains the supplementary crystallographic data for the complexes in this study. These data can be obtained free of charge from the Cambridge Crystallographic Data Center via www.ccdc.cam.ac.uk/data_request/cif

Formation of the β-CD–H_2acacnn host–guest complex

The absorption spectra of H_2acacnn (c = 1.0 μM) at pH 7 (Figure 2a) is characterized by a structureless band (λ_{max} = 326 nm). The presence of β-CD in increasing concentrations leads to a continuous blue shift (hypsochromic shift) of the band envelope centered at 326 nm to 324 nm (in 4.0 mM β-CD). This band is due to the $n \rightarrow \pi^*$ transition. Also, the increase in β-CD leads to a regular hyperchromic shift. When the addition of β-CD is continued, above 5 mM of β-CD, an abrupt increase in the absorbance (hyperchromic shift) could be observed. Above this concentration, there is another 2 nm blue shift of the band and a continuous but small hyperchromic shift.

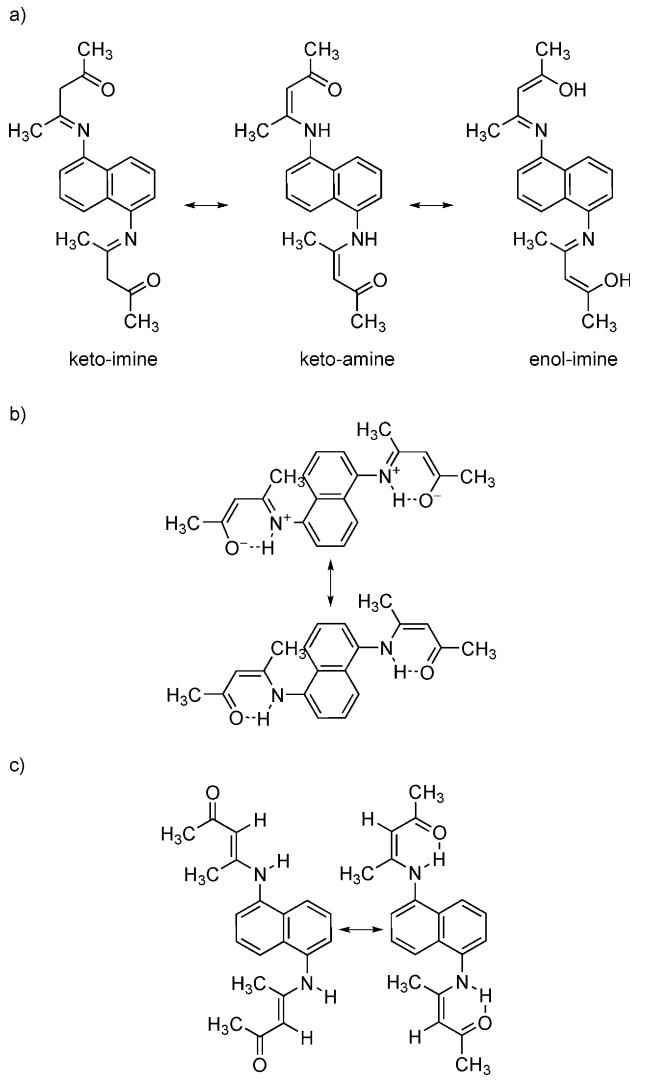

Scheme 1. a) Possible tautomers, b) ionic and hydrogen-bonding interactions, c) *E*, *Z* isomers of H_2acacnn.

The blue shift in absorbance is due to the change in the microenvironment of H_2acacnn in aqueous solution upon addition of β-CD. The host–guest association between β-CD and H_2acacnn leads to the shift since the hydrophobic cavity of β-CD offers an environment different from polar water molecules. The overall small shift of the absorption maximum suggests that there is no strong bonding between the H_2acacnn molecule and β-CD. The hyperchromic shift observed upon addition of β-CD is due to the free movement of electrons into various energy levels and the resulting enhanced absorption of UV light. This is a consequence of the molecular interaction between the β-CD and the H_2acacnn molecules, which induces structural modifications in the system. The electronic transition probability of the H_2acacnn electrons increases in the presence of β-CD; hence, the magnitude of absorbance and the molar absorption coefficient increase. The sheer change of absorbance above 5 mM β-CD implies that the electronic charge distribution and the associated transition moment of H_2acacnn are different on β-CD binding, compared with those observed in the preceding lower concentrations β-CD. Another important observation is that at higher concentrations of β-CD, the absorption spectra of H_2acacnn show a vivid isosbestic point at 352 nm which is due to the equilibrium between the free and the β-CD-bound H_2acacnn molecules in solution.

Aside from the absorption band at 326 nm, H_2acacnn shows another band at 211 nm, corresponding to the $\pi\rightarrow\pi^*$ transition. This band is structureless, probably due to the substitutions on the aromatic naphthalene ring. This band shows a bathochromic shift when β-CD is added in aliquots. At 5 mM β-CD, this shifted band is centered at 218 nm, while at 10 mM β-CD, it appears at 221 nm. Moreover, there is a continuous hyperchromic shift with increasing β-CD concentrations. The overall 10 nm bathochromic shift and the regular hyperchromic shift are attributed to the complex formation of H_2acacnn with β-CD. The red shift and the increase in intensity of this band can be related to the conformational stability of the substituent aminopentenone chains of H_2acacnn, attained due to the restriction offered by the encapsulating β-CD molecule. Presumably, the addition of β-CD results in the decrease in energy level of the excited state accompanying dipole-dipole interactions. Also, in the band corresponding to the $\pi\rightarrow\pi^*$ transition, the addition of β-CD shows two distinct sets of absorption trends, namely a regular hyperchromic shift up to 5 mM β-CD and an abrupt increase of absorbance followed by a regular hyperchromic shift above this concentration. Evidently, β-CD forms an inclusion complex with H_2acacnn, and there may be two different types of complexes formed. In order to evaluate the stoichiometry of the complex(es) and their binding strength(s), plots were made for the following binding event, assuming 1:1 stoichiometry:[29]

$$CD + H_2acacnn \leftrightarrow CD : H_2acacnn \quad (1)$$

$$K = \frac{CD : H2acacnn}{[CD][H2acacnn]} \text{ (or)}$$
$$[CD : H2acacnn] = K[CD][H_2acacnn] \quad (2)$$

where $[CD]_t = [CD] + [CD : H_2acacnn]$, (3)

$$[CD]_t = [CD] + K[CD][H_2acacnn], \quad (4)$$

$$[CD]_t = [CD](1 + K[H_2acacnn]), \quad (5)$$

$$[H_2acacnn]_t = [H_2acacnn] + [CD : H_2acacnn] \quad (6)$$

Substituting Equation 2 in Equation 6, we get

$$[H_2acacnn]_t = [H_2acacnn] + K[CD][\ H_2acacnn] \quad (7)$$

Substituting Equation 5 in Equation 7, we get

$$[H_2acacnn]_t = [H_2acacnn] + \frac{K[H2acacnn][CD]_t}{1 + K[H2acacnn]} \quad (8)$$

where CD, H_2acacnn, CD:H_2acacnn, H_2acacnn$_t$, and *K* are the free CD, the free H_2acacnn, the host–guest complex, the total H_2acacnn concentration, and the binding constant, respective-

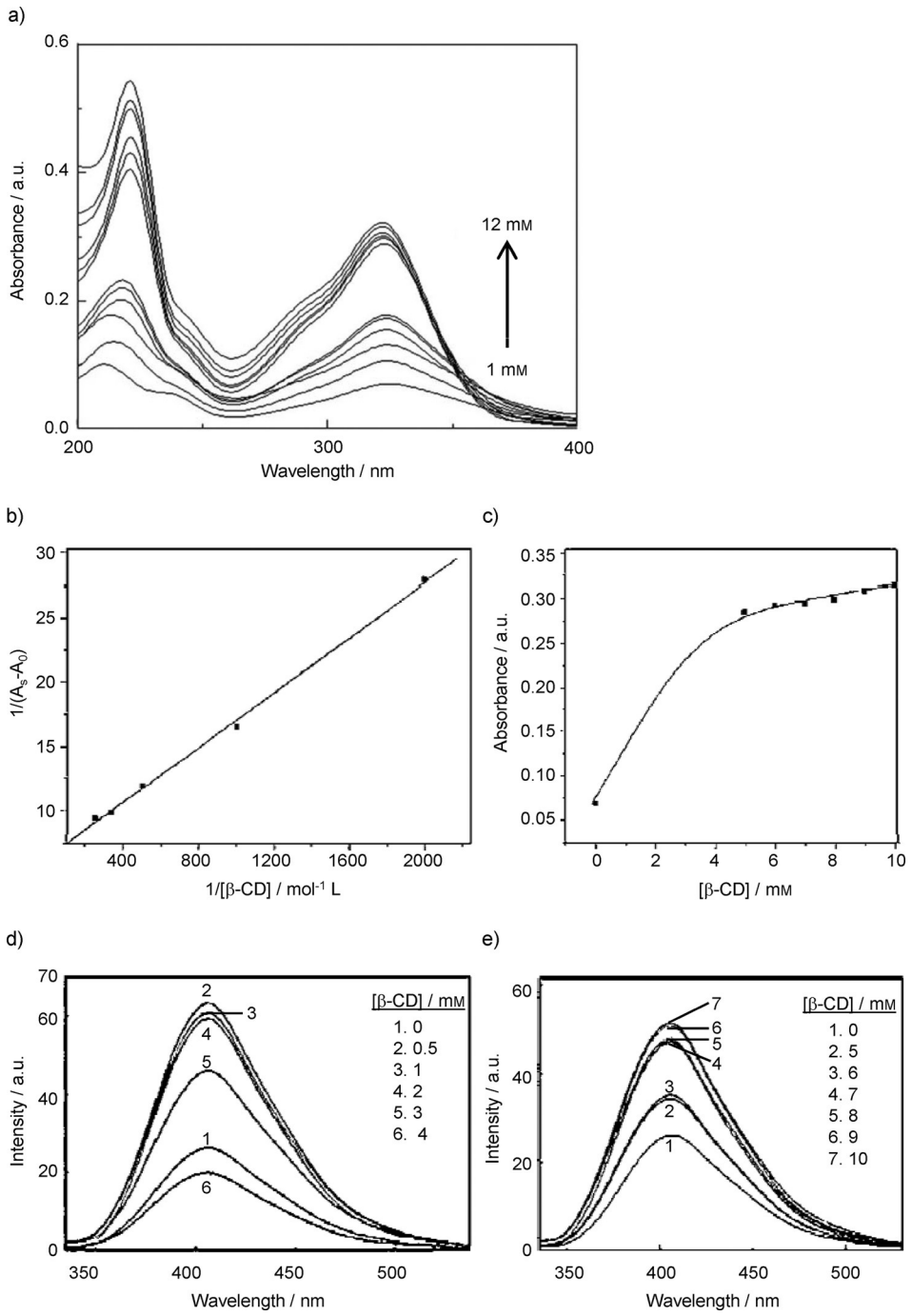

Figure 2. a) Absorption spectral changes of H_2acacnn upon binding to β-CD. Hyperchromic shift of the absorption band occurs at the addition of β-CD. b) Plot of $1/A_S-A_0$ vs. 1/[β-CD], made using the absorption spectral data of the binding titration. c) Nonlinear plot showing the absorption of H_2acacnn as a function of [β-CD]. d) Fluorescence spectral changes of H_2acacnn upon addition of β-CD in its lower concentration range. e) Enhancement of fluorescence upon addition of β-CD at its higher concentration range.

ly. Equation 8 predicts a linear correlation between $H_2acacnn_t$ and CD_t which is actually obtained within the concentration range of 0 to 5.0 mM β-CD (this is the highest concentration used in the plot). The linearity obtained in this plot (Figure 2b) suggests that at these lower concentration limits, there is formation of a 1:1 complex of β-CD:H_2acacnn. However, when the concentration higher than this range is included in the plot (the maximum concentration of β-CD is 10 mM), there is a deviation from linearity. Hence, a nonlinear plot is made (Figure 2c), for the higher order complex formed, considering two cases, namely 1:1 and 1:2 mixed complexes coexist [Eq. (9)] and only the 1:2 complex (H_2acacnn:β-CD) is formed [Eq. (10)].[30]

$$A = A_0 + \frac{A_1K_1[CD] + A_2K_1K_2[CD]_2}{1 + K_1[CD] + K_1K_2[CD]_2} \quad (9)$$

$$A = \frac{A_0 + A_2K_1K_2[CD]_2}{1 + K_1K_2[CD]_2} \quad (10)$$

where A_0, A_1, and A_2 are the absorbances of H_2acacnn in water, 1:1 H_2acacnn:β-CD complex, and 1:2 complex respectively. K_1 and K_2 indicate the binding constants of the 1:1 and 1:2 complexes. $[CD]_0$, the initial concentration, can be used to replace [CD], the equilibrium concentration, since it is much smaller than [CD]. Reasonable values of standard errors, correlation coefficient, and confidence intervals could be obtained only when a nonlinear regression analysis using Equation 10 was done.

The binding constants determined for the 1:1 and the 1:2 H_2acacnn:β-CD complexes are 606 M^{-1} and 2.32×10^5 M^{-2} respectively. The fitting procedure was done using the above equations in the region of maximum variation of absorbance changes (325 nm). These binding constant values are independent estimates of the ground state binding affinities of H_2acacnn with β-CD. The stepwise binding constants cannot be determined for the 1:2 complex from curve fitting done with just a single equation.

The fluorescence emission of H_2acacnn in water (at pH 7) is a structureless band with a maximum at 407 nm (Figure 2d). When β-CD is added in stepwise increasing concentrations, H_2acacnn is transferred from the aqueous bulk to the hydrophobic β-CD cavity, and the relative intensity of fluorescence reflects a change in the microenvironment of the guest mole-

cule. The fluorescence behavior of H_2acacnn is distinctly different between the two concentration ranges, namely 0 to 5 and 5 to 10 mM β-CD. The usual β-CD complex formation results in an enhancement of the guest fluorescence intensity owing to the steric hindrance, offered by the β-CD cavity, to the molecular degrees of freedom leading to a nonradiative deactivation of the singlet excited state. We observed an immediate enhancement of fluorescence of H_2acacnn at the first addition of β-CD (5.0 mM), followed by a quenching of fluorescence of the originally enhanced band continuously up to 4.0 mM of β-CD. This cannot be fitted by a quenching plot as the fluorescence intensity of H_2acacnn without β-CD lies below the fluorescence intensities of β-CD-bound H_2acacnn in the above-mentioned concentration range. Although the abrupt enhancement of fluorescence at the first addition can be easily understood, the subsequent quenching of fluorescence is unusual. The size match between the host cavity and the guest and the stoichiometry of the complex, to a specific microenvironment inside the β-CD cavity, can control such an effect. Generally, lower- or higher-order complexes govern respectively the less or more tightly binding behavior of the guest molecule with the β-CD environment. Moreover, in the higher order complexes, the guest is more protected from contact with water. The quenching of fluorescence may occur due to the low penetration of the host cavity by one side chain of the H_2acacnn molecule, leaving out the central naphthyl ring outside the host. Now, the aminopentenone chain, having sufficient conformational flexibility and a less restricted degree of freedom, cannot get induced in much variation of its emission. It is usual for a linear carbon chain to rattle around inside the β-CD cavity.[31] In general, the naphthalene ring can be included deeply into the β-CD cavity only with the long axis parallel to the CD axis.[5] In H_2acacnn, since the naphthyl ring is not parallel to the aminopentenone chain, it cannot be accommodated by β-CD.

With 5 to 10 mM of added β-CD, the H_2acacnn displays an enhancement of fluorescence (Figure 2e). Again, this enhancement of fluorescence is ascribed to the accommodation of the second aminopentenone chain into the next β-CD molecule. The fluorescence maximum is not significantly shifted. Since only the side chains of H_2acacnn are entering the β-CD cavity, water molecules can freely move through the cavity along the sides of the encapsulated part of H_2acacnn, resulting in the effective dielectric constant of the β-CD cavity to remain similar to that of water. This explains the insignificant shift of fluorescence maximum. Similar to the plot made using Equation 10 which utilizes absorbance, usually, we should be able to use the fluorescence intensity to do a nonlinear plot. However, in the case of H_2acacnn, the plot could not be made because initially, there is fluorescence quenching at the low concentration range of β-CD. Hence, mainly based on the results of UV/Vis absorption spectral data, it is inferred that H_2acacnn forms a higher order (1:2) complex with β-CD at higher concentrations of β-CD, with the β-CD molecules encapsulating the aminopentenone chains.

NMR spectral analysis

In order to obtain direct evidence for the formation of the host–guest complex and to provide additional and concrete evidence for the mode of inclusion discussed in the previous section, ^{1}H NMR spectra were recorded for the free H_2acacnn, the free β-CD, and the β-CD–H_2acacnn complex. The significant differences in the chemical shift values between these spectra confirm the formation of the inclusion complex. Larger and pronounced chemical shifts are observed for the H^3 and H^5 protons of β-CD, compared to H^2 and H^4 protons. The H^3 and H^5 protons are located inside the hydrophobic cavity of β-CD. The first inference is that the complex is formed between β-CD and H_2acacnn through the host–guest association. The H^2 and H^4 protons are on the outer surface of β-CD, hence their signals are less affected by the guest molecule. The chemical shifts of the protons of the free H_2acacnn and the β-CD–H_2acacnn host–guest complex are listed in SI 1 in the Supporting Information.

The geometry of the inclusion complex and the structural information was provided by rotating-frame Overhauser effect spectroscopy (ROESY). The distance between the nuclei that are interacting with each other is directly proportional to the intensities of the cross peaks in the ROESY spectrum. When the internuclear distance between protons decreases, the cross peak intensity decreases. The ROESY spectrum of the β-CD–H_2acacnn complex displays cross peaks between the protons lined inside the cavity of β-CD, namely H^3 and H^5, and the protons of the aminopentenone substituent of H_2acacnn shown as H^{25} and H^{26} in Figure 3a. There are two observations from these results: 1) the two aminopentenone chains are encapsulated by β-CD, forming a 1:2 complex, and 2) the cross peaks are intense and, hence, the alkenyl protons are well placed inside the β-CD cavity, close to its H^3 and H^5 protons. The other weak cross peaks between the secondary hydroxy proton signals of β-CD and the aromatic protons (H^4 and H^7) signals of H_2acacnn imply that the two β-CD molecules slide through the aminopentenone chains and get closer to the aromatic naphthyl ring although not encapsulating it. Very weak cross peaks are observed for the interaction between the end methyl protons of H_2acacnn (H^{17} and H^{23}) and the cavity protons of β-CD, suggesting that the methyl end group penetrates deeply and comes outside the β-CD cavity through the other rim, as shown in the schematic diagram of the 1:2 inclusion complex (Figure 3b).

We performed diffusion-ordered NMR spectroscopy (DOSY) for H_2acacnn and the β-CD–H_2acacnn complex (SI 2 in the Supporting Information) in order to demonstrate that the complex is stable and to calculate the binding constant. The diffusion coefficient of free H_2acacnn is $4.515\times10^{-10]}$ m^2s^{-1} and that of β-CD is 3.701×10^{-10} m^2s^{-1}. In the DOSY spectrum of β-CD–H_2acacnn complex, the signals due to the unbound H_2acacnn are not found suggesting that it is fully complexed to β-CD. The diffusion coefficient of β-CD is 3.254×10^{-10} m^2s^{-1}.[32] The application of DOSY data to the binding of H_2acacnn to β-CD gives a binding constant value of 512 M^{-1}, which indicates strong binding and good stability of the complex. It should be

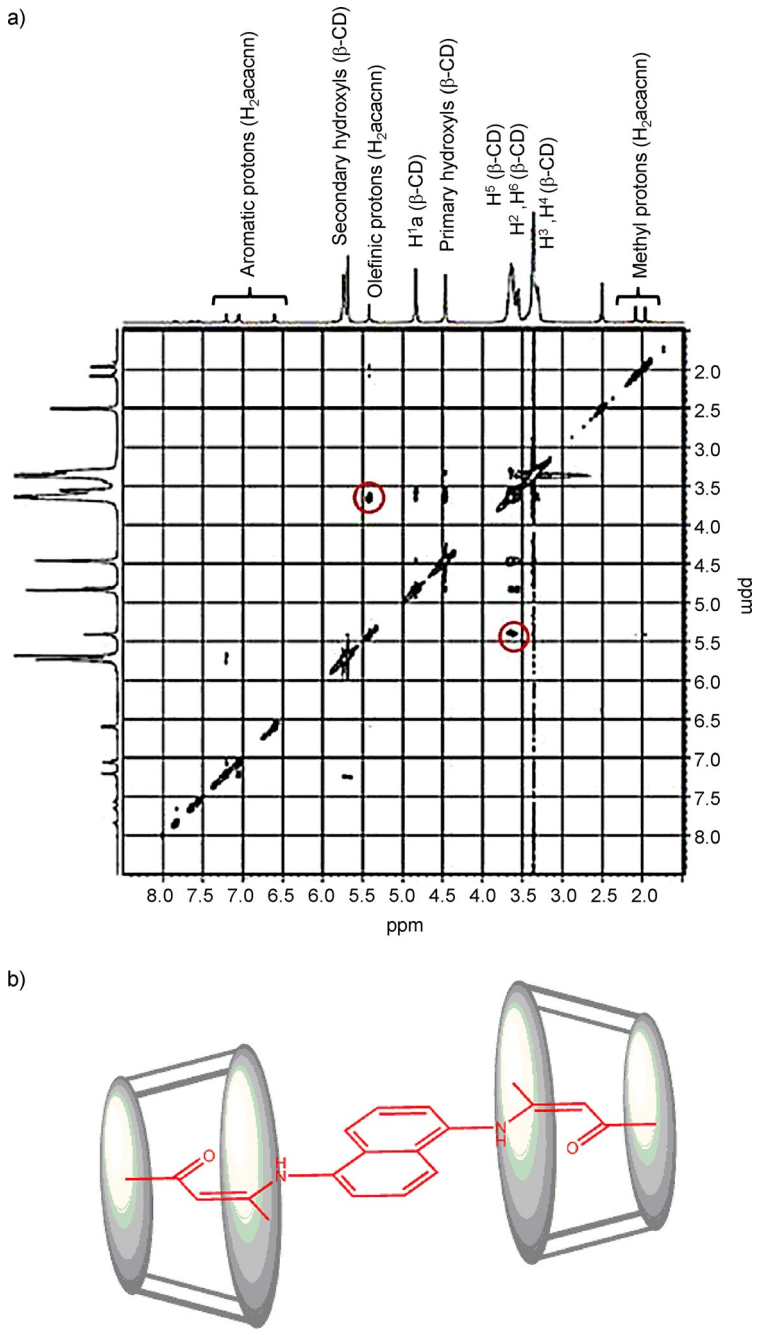

Figure 3. a) 2D ROESY spectrum of H_2acacnn–β-CD. The contours harmonize with the proton–proton proximities in the host–guest complex. b) Schematic representation of the mode of H_2acacnn–β-CD binding.

noted that this is close to the calculated value using the steady-state fluorescence spectral data.

Effect of pH on the absorption and fluorescence characteristics of H_2acacnn

The absorption and the fluorescence spectra of H_2acacnn are studied in the pH range of 1–7. With the decrease of pH from 7, the absorption spectrum of H_2acacnn (λ_{max} = 326 nm) is considerably blue shifted (SI 3a in the Supporting Information). Below pH 4.5, the 326 nm band disappears completely. Parallel to this observation, there is a corresponding increase of absorbance at 275 nm, with the formation of a new band at around 291–292 nm. A large blue shift of absorbance is characteristic of the formation of a cation due to the H^+ ions protonating the nitrogen attached to the aromatic ring of the naphthalene through its unshared pair of electrons. This leads to a shortening of the conjugation of electrons in the chromophore and, hence, to a blue shift of the absorbance band. The presence of an isosbestic point in the spectra indicates that there is an equilibrium existing between two forms of the H_2acacnn molecule, namely the neutral and the cationic forms. There is also another isosbestic point observed at 220–221 nm. The absorption spectrum of the protonated H_2acacnn resembles the spectrum of the unsubstituted naphthalene.[33] This result suggests that the amino nitrogens attached to the naphthalene are protonated at a low pH, decreasing the conjugation of electrons and the length of the chromophore. The ground state pK_a of this equilibrium in solution is calculated as follows:

$$C_1 = \frac{A(\lambda_1)\varepsilon_2(\lambda_2) - A(\lambda_2)\varepsilon_2(\lambda_1)}{\varepsilon_2(\lambda_1)\varepsilon_2(\lambda_2) - \varepsilon 1(\lambda_2)\varepsilon_2(\lambda_1)} \quad (11)$$

$$C_2 = C_T - C_1 \quad (12)$$

$$pK_a = pH + \log C_1/C_2 \quad (13)$$

In the above equations, C_T represents the total concentration of H_2acacnn in neutral and cationic forms and $\varepsilon_1(\lambda_1)$, $\varepsilon_2(\lambda_2)$, $\varepsilon_2(\lambda_1)$, $\varepsilon_2(\lambda_2)$ are the molar extinction coefficients of the protonated and neutral forms at the two different wavelengths λ_1 and λ_2, respectively (275 nm and 325 nm in this case). The calculated pK_a for the neutral-cation equilibrium of H_2acacnn in water, calculated using the above equations, is 3.7 ± 0.2.

The effect of acid strength on the absorption spectrum of H_2acacnn is shown in SI 3b in the Supporting Information. The longer wavelength absorption band (325 nm) decreases in absorbance with a corresponding increase at a shorter wavelength (230 nm). There is an isosbestic point observed in the range of 268 to 272 nm, which is not as clear as obtained for the prototropic equilibrium of H_2acacnn in water. This may be due to the presence of β-CD. The ground state pK_a value of H_2acacnn in the presence of β-CD was determined in the spectrophotometric method as 3.5 ± 0.2. This value is slightly lower than the pK_a obtained for the same equilibrium in water (3.7 ± 0.2), which is due to the hindrance offered by the β-CD molecule as it covers up the aminopentenone chains of H_2acacnn.

The fluorescence spectra of H_2acacnn in water, at various pH levels, are shown in SI 3c in the Supporting Information. The fluorescence spectra were recorded with excitation at the isosbestic points. When the pH is reduced from 7, the fluorescence emission band at 411 nm starts to quench with a red

shift of fluorescence. The decrease of intensity at this wavelength is accompanied by a corresponding increase in intensity at a longer wavelength. The band at 411 nm completely disappears in the pH range below 5. The new band formed is centered at 454 nm. This band is formed due to the protonation of the H_2acacnn molecule. There is an isoemissive point around 420 nm, indicating that there exists a prototropic equilibrium between the neutral and the protonated forms of H_2acacnn. The fluorimetric titration curves plotted as I/I_0 versus pH at the wavelengths 411 nm and 454 nm are sigmoidal, and these intersect at the middle of inflection. This is due to the occurrence of a single phenomenon, that is, the protonation of H_2acacnn. The pK_a^* value (the excited-state pK_a) of the neutral-cation equilibrium of H_2acacnn could be directly obtained from the intersection of the fluorimetric titration curves, and the observed value is 3.4 ± 0.2.

A similar pH-based fluorimetric titration was done with H_2acacnn in the presence of β-CD (SI 3d in the Supporting Information). A red shift of the fluorescence band of the neutral form is observed on decreasing the pH below 7, which is similar to the observation of the fluorescence shift of H_2acacnn in water. However, the newly formed red-shifted band, which corresponds to the protonated form of H_2acacnn, is more intense than the fluorescence band of the neutral form. There is no single isoemissive point albeit most of the spectra, in the studied pH range, passes through a meeting point at around 395 nm. The absence of a clear isoemissive point may be due to two reasons: 1) the proton that tends to add to the nitrogen lone pair of the substituent on H_2acacnn might be in equilibrium between its different tautomeric forms and 2) the β-CD covers one of the aminopentenones at this concentration (4.0 mM); and so there may be two nonuniform sites of protonation, in the sense that the nitrogen of one of the aminopentenones is open and the other is β-CD-encapsulated. The excited-state pK_a calculated for H_2acacnn in the presence of β-CD was calculated from the fluorimetric titration curves in the plot of I/I_0 versus pH as 3.2 ± 0.2.

Binding of H_2acacnn to DNA

The interaction of H_2acacnn with calf thymus DNA was studied by using absorption and fluorescence spectroscopy. The binding titration was carried out by keeping the concentration of H_2acacnn constant at 1.0 μM and adding aliquots of DNA. The absorption spectra of H_2acacnn with the various added amounts of DNA are shown in Figure 4a. The range of concentration of the added DNA is 0–1.4 μM. With an increase in the concentration of DNA, the absorbance of the 322 nm band decreases along with a hypsochromic shift of about 2 nm. The lesser availability of the H_2acacnn molecule to the surrounding solvent molecules, due to binding to DNA, results in the decrease in absorbance. The hypsochromic shift may be due to the intercalation of the naphthalene moiety of H_2acacnn into the DNA helix. A decrease in absorbance is an indication of the close proximity of the small molecule (H_2acacnn) to the DNA bases.[34] Moreover, hypsochromism is generally a result of the contraction of the helical axis of the DNA and a change of conformation of DNA.[35] On the other hand, damage to the DNA double helix would result in a hyperchromic shift of absorbance. We do not observe such a hyperchromism; hence, it can be inferred that there is no damage to the DNA upon H_2acacnn binding. Further evidence for intercalative binding is discussed in the section on molecular docking. A double recip-

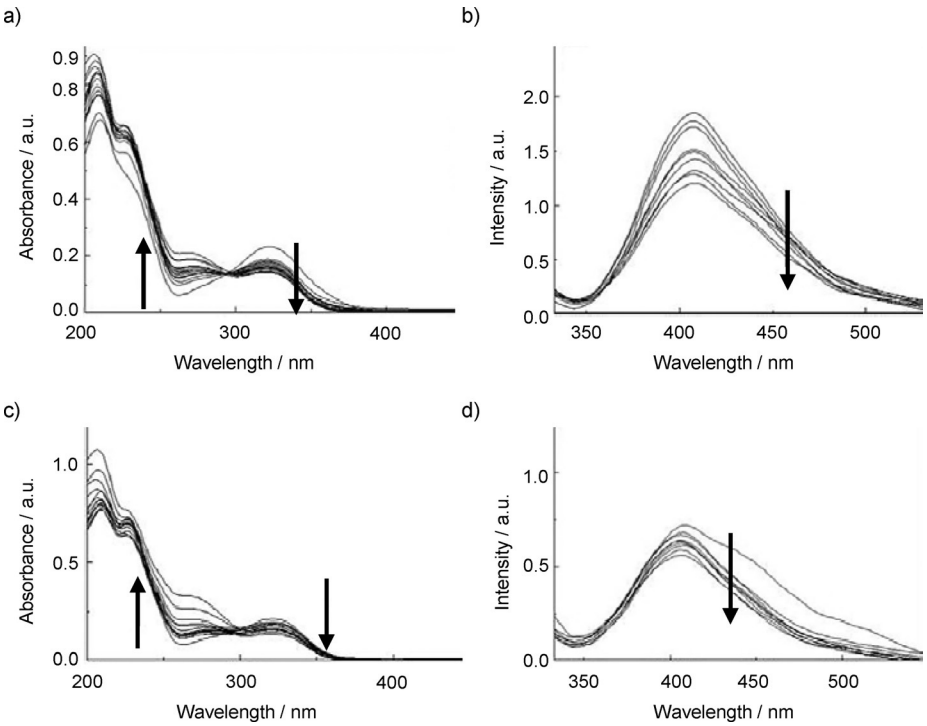

Figure 4. a) Absorption spectra of H_2acacnn with various amounts of DNA ([H_2acacnn] = 1 μM, [DNA] varied from 0–1.4 μM in increments of 0.1). b) Fluorescence spectral changes upon addition of DNA to H_2acacnn ([DNA] varied: 0, 0.1, 0.2, 0.4, 0.6, 0.8, 1.0, 1.2, and 1.4 μM). c) Absorption titration of the H_2acacnn–β-CD–DNA binding ([β-CD] = 12 mM). d) Fluorescence titration of the H_2acacnn–β-CD–DNA binding.

rocal plot was used to determine the binding constant of the H_2acacnn–DNA binding using the following equation:[36]

$$\frac{A_0}{A - A_0} = \frac{\varepsilon_{H2acacnn}}{\varepsilon_{H2acacnn-\beta-CD} - \varepsilon_{H2acacnn}} + \frac{\varepsilon_{H2acacnn}}{(\varepsilon_{H2acacnn-\beta-CD} - \varepsilon_{H2acacnn})K_b[DNA]} \quad (14)$$

where A_0 and A are the absorbances of the free H_2acacnn in water and at various concentrations of the added DNA and $\varepsilon_{H2acacnn}$ and $\varepsilon_{H2acacnn-\beta-CD}$ are the corresponding absorption coefficients. The linear plot of $A_0/A-A_0$ versus 1/[DNA] (correlation coefficient, 0.99) is shown in SI 4a in the Supporting Information. The calculated binding constant K_b is 2.09×10^5 M^{-1}.

The H_2acacnn–DNA binding was also studied using fluorescence spectroscopy. The fluorescence titration of H_2acacnn with DNA shows a quenching of fluorescence (Figure 4b), along with a significant blue shift of the band at 407 nm. The Stern–Volmer quenching constant (K_{SV}) is calculated from the plot (SI 4b in the Supporting Information) made using the fluorescence titration data following the equation:[37]

$$\frac{F_0}{F} = 1 + K_{SV}[Q] = k_q\tau_0[Q] \quad (15)$$

where F_0 and F are the intensities of fluorescence of H_2acacnn in the absence and the presence of DNA, k_q is the bimolecular quenching constant, τ_0 is the fluorescence lifetime of H_2acacnn, and [Q] is the concentration of the quencher (DNA). The K_{SV}, which is proportional to the quenching efficiency of DNA, is 3.75×10^4 M^{-1}.

The binding data were cast into a plot of log (F_0/F−F) versus log [Q], where F_0 is the fluorescence intensity of H_2acacnn with no added quencher and F is the fluorescence intensity at each concentration of the quencher. They were straight-line-fitted (SI 4c in the Supporting Information) to the model:[38]

$$\log\left(\frac{F_0}{F} - F\right) = \log K_b + n\log[Q] \quad (16)$$

where n is the number of binding sites, [Q] is the concentration of the quencher (DNA), and K_b is the binding constant.

The influence of β-CD encapsulation on the binding of H_2acacnn with DNA was studied using the titration of H_2acacnn–β-CD complex against DNA. H_2acacnn–β-CD exhibits absorption bands with λ_{max} at 209, 228, and 321 nm (Figure 4c). Stepwise addition of DNA up to 1.4 μM results in the hypsochromic shift of absorbance along with a small blue shift. In the presence of β-CD, H_2acacnn is less available for energy transfer to the surrounding solvent molecules than in pure water. This leads to a decrease in the absorbance of H_2acacnn. The naphthalene moiety of H_2acacnn may have intercalated into the DNA helix as the competitive binding between cyclodextrin–H_2acacnn and DNA–H_2acacnn takes place, where the fluorophore sheds the two cyclodextrin units in favor of the DNA. The calculated binding constant is 5.67×10^3 M^{-1}. The binding constant reported for the 1:2 complex with DNA is nearly the same value as the binding constant for the DNA–H_2acacnn complex divided by the 1:1 β-CD–H_2acacnn binding constant. The reciprocal plot showing the relative changes of absorbance of H_2acacnn–β-CD complex with variation in the DNA concentration is given in SI 4d in the Supporting Information. A decrease of binding constant of the binding interaction between H_2acacnn and DNA in the presence of β-CD was observed. A similar binding titration between H_2acacnn–β-CD and DNA was also done using fluorescence spectroscopy (Figure 4d). The addition of DNA to the β-CD-bound H_2acacnn leads to a quenching of fluorescence, and the Stern–Volmer plot of the quenching is shown in SI 4e in the Supporting Information. The K_{SV} is 1.74×10^4 mol^{-1} L. The binding constant determined for the binding of H_2acacnn–β-CD to DNA is 2.07×10^2 M^{-1}, using the plot as in SI 4f in the Supporting Information. The mode of binding of H_2acacnn to DNA can be visualized as given in Scheme 2.

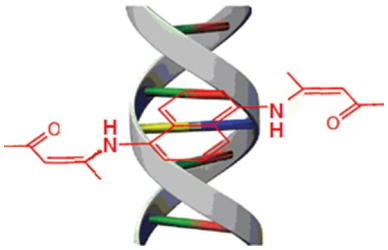

Scheme 2. Pictorial representation of the H_2acacnn–DNA association.

Molecular docking

The interaction profile of β-CD with H_2acacnn shows the existence of hydrogen, electrostatic, and hydrophobic interactions SI 5a in the Supporting Information. The interaction provides a the glide score of −1.99 kcal mol^{-1} at the binding site, aminopentenone moiety of H_2acacnn, and the secondary hydroxy groups of β-CD through the hydrogen bonds with the bond distances of 2.42 Å and 1.96 Å. The entry of the aminopentenone moiety of H_2acacnn into the hydrophobic cavity of β-CD is shown in Figure 3b. This observation is in accordance with the experimental binding studies. The types of interactions of H_2acacnn with DNA and the hydrogen bond length are given in SI 5 in the Supporting Information. H_2acacnn provides the best glide score with a G-score of −1.99 kcal mol^{-1} for binding to β-CD and −3.67 kcal mol^{-1} for binding to DNA. H_2acacnn is found to interact with DNA in two different sites by means of hydrogen bonding with a bond length of 2.113 Å and 9.068 Å in both the A and B-chains of DNA. The docked structure is shown in SI 5b in the Supporting Information. The mode of binding is pictorially represented in Scheme 2.

Logic gates

In Figure 5a, the change of absorbance of H_2acacnn with the concentration of protons and β-CD is represented. The absorbances at 235 nm and 215 nm are considered as output 1 and 2 respectively. When the pH is 6, that is, when the proton con-

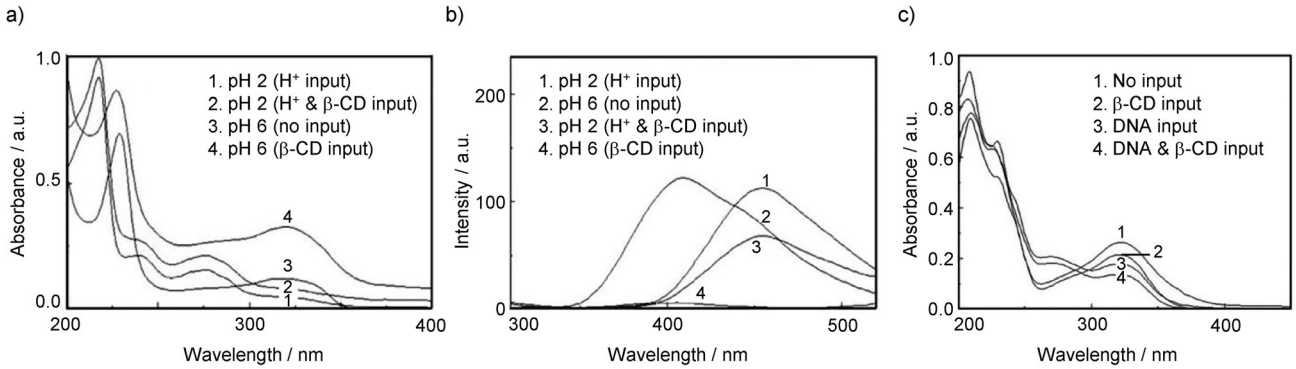

Figure 5. a) Change of absorption spectrum of H_2acacnn with the addition of protons and β-CD. b) Fluorescence spectra of H_2acacnn in its various forms. c) Change of absorption spectrum of free and β-CD-bound forms of H_2acacnn upon DNA binding.

centration of the solution is relatively less, the absorbance of H_2acacnn at 235 nm stands below the set-up threshold value of 0.8. This is a condition when no input, either H^+ or β-CD, is given. Addition of a proton shifts the absorbance to above the threshold level at λ_{235} and λ_{215} (a condition, ON) due to the protonation of H_2acacnn. In the presence of β-CD, the neutral form of H_2acacnn shows an absorbance greater than the threshold limit at λ_{235} and smaller at λ_{215}. The protonated H_2acacnn in the presence of β-CD shows OFF and ON signals at λ_{235} and λ_{215}, respectively. Hence, the system functions as a two-input XOR logic gate at λ_{235} and as a Buffer at λ_{215}. The truth table listing the inputs and outputs is represented in Figure 6a.

Figure 5b shows the fluorescence spectra of H_2acacnn in its various forms viewed as operating logic gates at λ_{400} and λ_{450}. With the threshold intensity set-up at 100, and considering the inputs as H^+ and β-CD, the output 1 (λ_{400}) results in a digital 1 (or ON) initially when there is no input, and in a digital 0 (or OFF) when the inputs are either H^+, β-CD, or both. This suggests that H_2acacnn can function as a NOR logic gate at λ_{400}. Similarly, at λ_{450}, the output 2 is a digital 1 when the input is H^+ alone, whereas in all the other conditions as shown in Figure 5b, it is a digital 0. The truth table and the logic gates are shown in Figure 6b. Hence at λ_{450}, the system operates as an INHIBIT logic gate. Considering the same fluorescence spectra of H_2acacnn with the same inputs, but having the threshold set at the intensity of 50 units, the digital output at λ_{450} shows the function as a Buffer as opposed to the INHIBIT logic gate observed when the threshold value is 100 (discussed above). However, at λ_{400}, NOR gate operations are observed regardless of the threshold intensity of fluorescence. Figure 6c shows the truth table and the logic gate symbols corresponding to the above logic operations using fluorescence with threshold intensity value 50.

Considering the absorbances of the free- and the β-CD-bound H_2acacnn interacting with DNA [Figure 5c], the changes are monitored in the view of digital outputs. The inputs 1 and 2 are β-CD and calf thymus DNA respectively. The outputs are read out at λ_{265} and λ_{325}. With no inputs or with single input of β-CD, the output 1 (at λ_{265}) is a digital 0. With a single input of DNA alone, or β-CD/DNA, the output 1 is a digital 1. Hence at λ_{265}, the operation of a Buffer gate is observed. At λ_{325}, the output 2 is a digital 1 when there is no input or there are the inputs of β-CD or DNA alone. When both β-CD and DNA are the inputs, the output 2 is a digital 0. Hence, it is an operation of a NAND logic gate at λ_{325}. The truth table and the symbols of the two-input logic gates are given in Figure 6d.

Cancer cells show an aberrant regulation of hydrogen ion dynamics. This results in a reversal of the intracellular to extracellular pH gradient in cancer cells as compared to normal cells. This perturbation in pH dynamics rises very early in carcinogenesis and is one of the most common pathophysiological hallmarks of tumors.[39] In such a condition, the operation of the logic gates discussed above is relevant in the sense that H^+ ions are involved in the pH-dependent signal on–off switching of the H_2acacnn absorption and fluorescence, and β-CD can mimic the movement-restricted microenvironment of tumors. Moreover, a frequently used method for anticancer treatment is the application of a drug that binds to DNA, which affects cell proliferation. β-CD can tune the drug binding to DNA,[39] and the small molecule–DNA–β-CD chemical equilibrium can be mimicked by the logic gates discussed in the preceding paragraphs involving DNA and β-CD.

Conclusions

In the (*Z*)-5-(5-((*Z*)-4-oxopent-2-en-2-ylamino)naphthalen-1-ylamino)pent-3-en-2-one (H_2acacnn) crystal, the terminal moieties are oriented along the NH-substituted naphthyl rings. β-Cyclodextrin forms a 1:2 inclusion complex with H_2acacnn. Fluorescence enhancement on the complex formation occurs at a higher concentration range of β-CD. The aminopentenone chains of H_2acacnn are encapsulated by β-CD. In the lower concentration range of β-CD, since only one aminopentenone chain (which does not match the cavity size) gets into the host cavity, the complex gets greatly stabilized only at the formation of the 1:2 complex. The naphthyl rings are not encapsulated by β-CD as it can approach the rings only by sliding over the aminopentenone chains. The methyl end groups of the chains come outside the narrower rim of β-CD after entering through the larger rim. The pK_a value of H_2acacnn is very slightly different between the measurements in water and in

a)

INPUT		OUTPUT	
A (H^+)	B (β-CD)	X (235 nm)	Y (215 nm)
0	0	0	0
1	0	1	1
0	1	1	0
1	1	0	1

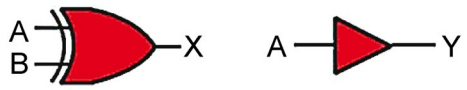

X = A XOR B Y = A

b)

INPUT (Threshold: 100)		OUTPUT	
A (H^+)	B (β-CD)	X (400 nm)	Y (450 nm)
0	0	1	0
1	0	0	1
0	1	0	0
1	1	0	0

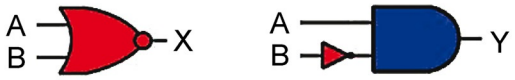

X = A NOR B INH

c)

INPUT (Threshold: 50)		OUTPUT	
A (H^+)	B (β-CD)	X (400 nm)	Y (450 nm)
0	0	1	1
1	0	0	1
0	1	0	0
1	1	0	1

X = A NOR B Y = (NOT B) OR A

d)

INPUT		OUTPUT	
A (DNA)	B (β-CD)	X (265 nm)	Y (325 nm)
0	0	0	1
1	0	1	1
0	1	0	1
1	1	1	0

X = A Y = A NAND B

Figure 6. Truth tables showing various logic gates. a) Results of the absorption spectra (threshold absorbance: 0.8). b) Results of the fluorescence spectra (threshold intensity: 100). c) Results of the fluorescence spectra (threshold intensity: 50). d) Results of the absorption spectra (threshold absorbance: 0.15).

aqueous β-CD media. The case is similar for the excited-state pK_a, and this means that the prototropic equilibrium is attained in the ground state and does not greatly vary in the excited state.

The system is suitable for functioning as a reliable logic gate platform as the binding to either β-CD or DNA is sufficiently strong. Binding to β-CD and to DNA results in the possible operation of different logics, and this can be related to the different modes of binding in these events and to the types of bonding and hydrophobic interactions involved. These signaling differences are relevant in human pathophysiological conditions. Both universal gates (NAND, NOR) and basic logical operators (Buffer, INHIBIT) are possible with this simple naphthalene-derivative-based molecular logic substrate. In mimicking the molecular scale biodynamics, this approach based on binding events is advantageous over photochemical switching due to its photostationary state dependence and the laggardness of the latter.

Experimental Section

Chemicals and preparation of solutions

Analytical-reagent-grade β-CD (Sigma–Aldrich) and calf thymus DNA (Genei, India) were used as received. The purity of DNA was tested before the spectral studies. The absorbance ratio (A_{260}/A_{280}) of DNA was greater than 1.8. The pH of the solutions was adjusted using a phosphate buffer, and the lower pH solutions (< pH 2) were prepared according to the modified Hammett's acidity scale using sulfuric acid.[28] Spectral grade solvents were used as received.

Stock solutions of H_2acacnn and β-CD were prepared in MeOH and triple-distilled H_2O, respectively. The stock solution of DNA was made in 50 mM of NaCl. Test solutions of H_2acacnn in H_2O/β-CD were prepared at pH 7 for the study of the inclusion complex formation. All the test solutions contained H_2acacnn in 1% MeOH (*v*/*v*) according to its appropriate dilution. Aliquots of DNA used for the DNA–H_2acacnn binding studies were made at pH 7 by diluting the stock solution. The experiments were done at 25 ± 2 °C. All the test solutions were homogeneous after the addition of the respective additives.

Instruments and recording of spectra

UV/Vis and fluorescence spectra were recorded using a double-beam Jasco V630 spectrophotometer (Mary's Court, USA) and a PerkinElmer LS55 spectrofluorometer (Waltham, USA), respectively. To record the spectra, cuvettes of path length 1 cm were used. The spectrofluorometer used a 120 W xenon lamp as the excitation source, and the excitation and emission bandwidths were fixed at 4 nm. pH was measured using an Elico LI 120 pH meter (Hyderabad, India). The absorption spectra were recorded against appropriate reference solutions which did not contain H_2acacnn.

Microanalysis of the complexes was done using a PerkinElmer PE 2400 series II CHNS/O elemental analyzer. Infrared (IR) spectra were recorded using KBr pellets (1% *w/w*) on a PerkinElmer Spectrum GX FT-IR spectrophotometer. Electronic spectra were recorded on a Shimadzu UV 3101PC spectrophotometer (Kyoto, Japan). Mass spectrometric analysis was performed using an electron spray ionization (ESI) technique on an LC Waters Q-TOF-micro mass spectrometer (Milford, USA) (spectrum shown in SI 6 in the Supporting Information). ^{1}H NMR spectra were recorded on a Bruker Avance II 200 FT-NMR spectrometer (Billerica, USA). Chemical shifts for proton resonances are reported in ppm (δ) relative to tetramethyl silane (TMS). The 2D-ROESY spectrum (of H_2acacnn-β-CD complex) was recorded on a Bruker AV III spectrometer. The operating frequency was 500 MHz, and the solvent used was [D6] DMSO. The mixing-time ROESY spectrum was 200 ms under spin lock conditions. DOSY NMR experiments were carried out using a Bruker AV III spectrometer equipped with a pulsed-gradient unit. The operating frequency was 400 MHz with a diffusion time of 180 μs and the gradient pulse of 1500 μs. The pulsed-gradient unit produced magnetic field gradients of 55 G cm^{-1} in the *z*-direction. The solvent used was $CDCl_3$. The pulse sequence used was a bipolar pulse longitudinal eddy current delay (BPLED) sequence. The gradient strength (*g*) was increased from 2 to 95% of the maximum in a quadratic ramp.

Preparation of H_2acacnn

Naphthalene 1,5-diamine (0.002 mol), acetylacetone (0.002 mol), and few drops of 6.2 M HOAc were mixed in EtOH (50 mL) and stirred constantly at reflux for 3 h and cooled to rt. The mixture was slowly evaporated in vacuo at rt for 48 h to afford yellowish-brown crystals (309 mg, 96%); ^{1}H NMR ($CDCl_3$, 500 MHz): $\delta = 12.78$ (broad s, NH, 2H), 7.97, 7.95 (d, $J = 10$ Hz, Ar–CH, 2H), 7.52, 7.50, 7.49 (t, $J = 10$ Hz, 5 Hz, Ar–CH, 2H), 7.32, 7.31 (d, $J = 5$ Hz, Ar–CH, 2H), 5.32 (s, =CH, 2H), 2.17 (s, CH_3, 6H), 1.89 ppm (s, CH_3, 6H); IR (KBr): $\tilde{\nu} = 4000$—3600 (br), 3500 (br), 2995, 1604, 1573, 1516, 1433, 1355, 1274, 1020, 956, 788 cm^{-1}; ESI-MS *m/z* $[M+1]^+$calcd for $C_{20}H_{22}N_2O_2$: 322.40, found 323.56; Anal. calcd for $C_{20}H_{22}N_2O_2$: C 74.51, H 6.88, N 8.69, found: C 74.72, H 6.59, N 8.78.

Single-crystal X-ray analysis

A crystal of suitable size was selected and mounted on the tip of a glass fiber and cemented using epoxy resin. Intensity data for the crystal was collected using Mo-K_α ($\lambda = 0.71073$ Å) radiation on a Bruker SMART APEX diffractometer equipped with CCD area detector. The hydrogen atom H^{1}N, which is bound to the nitrogen atom N^1, was located in the difference Fourier synthesis, and was refined semifreely with the help of a distance restraint, while constraining its *U*-value to 1.2 times the *U(eq)* value of N^1. All other hydrogen atoms were placed in calculated positions and refined by using a riding model.

Molecular docking

The structure of calf thymus DNA was retrieved from the RCSB Protein Data Bank (PDB) based on resolution of the structure, experimental feasibility by matrix data, comparative value of crystallographic model, and X-ray diffraction data.[40] A 10% removal of data for the structure observed and a comparison of 90% of the structure with the crystallographic model yielded the module structure. Docking was performed using Maestro v. 9.6 software (Schrodinger, New York, USA) to optimize the interaction of H_2acacnn with β-CD and calf thymus DNA. The structure of β-CD was built and optimized by molecular mechanics. The structure of calf thymus DNA was downloaded from the PDB (ID No. 3GJH)[40] and preprocessed prior to docking. The DNA grid was set up and generated from the receptor grid generation panel.

Acknowledgements

The authors would like to thank Dr. Paul Dhinakaran, Chancellor, and Dr. S. Sundar Manoharan, the Vice Chancellor of Karunya University, for their efforts in forming the new lab. They also thank the Sophisticated Analaytical Instrument Facility of the Indian Institute of Science (SAIF IISc), Bangalore, for assistance in recording ROESY and DOSY NMR spectra. M.S.P. is thankful to the German Academic Exchange Service (DAAD) for the opportunity to visit Prof. Werner R Thiel's lab at the Kaiserslautern University of Technology, Germany and to the Science and Engineering Research Board (SERB), Department of Science and Technology, India, for the financial support (project number SB/FT/CS-068/2012).

Keywords: β-cyclodextrin · fluorescence spectroscopy · host—guest interaction · molecular logic gates · naphthalene · supramolecular chemistry

[1] E. B. Tjaden, D. C. Swenson, R. F. Jordan, J. L. Peterson, *Organometallics* **1995**, *14*, 371 – 386.
[2] a) C.-H. Xu, W. Sun, Y.-R. Zheng, C.-J. Fang, C. Zhou, J.-Y. Jin, C.-H. Yan, *New J. Chem.* **2009**, *33*, 838 – 846; Fang, C. Zhou, J.-Y. Jin, C.-H. Yan, *New J. Chem.* **2009**, *33*, 838 – 846; b) S. Kou, H. N. Lee, D. van Noort, K. M. K. Swamy, S. H. Kim, J. H. Soh, K.-M. Lee, S.-W. Nam, J. Yoon, S. Park, *Angew. Chem. Int. Ed.* **2008**, *47*, 872 – 876; *Angew. Chem.* **2008**, *120*, 886 – 890; c) X. Zhou, X. Wu, J. Yoon, *Chem. Commun.* **2015**, *51*, 111 – 113; d) X.-Y. Liu, X. Han, L.-P. Zhang, C.-H. Tung, L.-Z. Wu, *Phys. Chem. Chem. Phys.* **2010**, *12*, 13026 – 13033.
[3] a) K. Szacilowski, *Infochemistry – Information Processing at the Nanoscale*, John Wiley & Sons, Chichester, **2012**; b) A. P. de Silva, *Molecular-logic Based Computing*, RSC Publishing, Cambridge, **2013**; c) *Molecular and Supramolecular Information Processing – From Molecular Switches to Unconventional Computing* (Ed.: E. Katz), Wiley-VCH, Weinheim, **2012**.
[4] See OPTI-CCA under http://www.osmetech.com/opti/index.html.
[5] A. P. de Silva, D. B. Fox, T. S. Moody, S. M. Weir, *Trends Biotechnol.* **2001**, *19*, 29 – 32.
[6] R. Y. Tsien, *Am. J. Physiol.* **1992**, *263*, C723 – C728.
[7] D. Melnikov, G. Strack, J. Zhou, J. R. Windmiller, J. Halámek, V. Bocharova, M.-C. Chuang, P. Santhosh, V. Privman, J. Wang, E. Katz, *J. Phys. Chem. B* **2010**, *114*, 12166 – 12174.
[8] W. Gao, L. Zhang, Y.-M. Zhang, R.-P. Liang, J.-D. Qiu, *J. Phys. Chem. C* **2014**, *118*, 14410 – 14417.
[9] T. Konry, D. R. J. Walt, *J. Am. Chem. Soc.* **2009**, *131*, 13232 – 13233.
[10] S. Angelos, Y. W. Yang, N. M. Khashab, J. F. Stoddart, J. I. Zink, *J. Am. Chem. Soc.* **2009**, *131*, 11344 – 11346.

[11] G. Mayer, A. Heckel, *Angew. Chem. Int. Ed.* **2006**, *45*, 4900 – 4921; *Angew. Chem.* **2006**, *118*, 5020 – 5042.
[12] D. Tong, H. Duan, H. Zhuang, J. Cao, Z. Wei, Y. Lin, *RSC Adv.* **2014**, *4*, 5363 – 5366.
[13] S. Ozlem, E. U. Akkaya, *J. Am. Chem. Soc.* **2009**, *131*, 48 – 49.
[14] J. A. Goode, D. J. Chadwick, *The Tumor Microenviroment: Causes and Consequences of Hypoxia And Acidity*, John Wiley & Sons, Inc., New York, NY, **2001**.
[15] P. Montcourrier, P. H. Mangeat, C. Valembois, G. Salazar, A. Sahuquet, C. Duperray, H. Rochefort, *J. Cell Sci.* **1994**, *107*, 2381 – 2391.
[16] M. Pita, V. Privman, M. A. Argula, D. Melnikov, V. Bocharova, E. Katz, *Phys. Chem. Chem. Phys.* **2011**, *13*, 4507 – 4513.
[17] I. V. M. V. Enoch, M. Swaminathan, *J. Chem. Res.* **2006**, *2006*, 523 – 526.
[18] J. M. C. Xavier, S. Chandrasekaran, V. Gunasekaran, I. V. M. V. Enoch, V. Gunasekaran, *Appl. Spectrosc.* **2013**, *67*, 1042 – 1048.
[19] N. Basílio, A. Fernandes, V. de Freitas, S. Gago, F. Pina, *New J. Chem.* **2013**, *37*, 3166 – 3173.
[20] R. N. Dsouza, U. Pischel, W. M. Nau, *Chem. Rev.* **2011**, *111*, 7941 – 7980.
[21] A. Chatterjee, B. Maity, D. Seth, *RSC Adv.* **2014**, *4*, 13989 – 14000.
[22] A. K. Mandal, P. Das, P. Mahato, S. Acharya, A. Das, *J. Org. Chem.* **2012**, *77*, 6789 – 6800.
[23] X. Meng, W. Zhu, Q. Zhang, Y. Feng, W. Tan, H. Tian, *J. Phys. Chem. B* **2008**, *112*, 15636 – 15645.
[24] T. S. Anirudhan, A. M. Mohan, *RSC Adv.* **2014**, *4*, 12109 – 12118.
[25] T. Zhang, S. Sun, F. Liu, Y. Pang, J. Fan, X. Peng, *Phys. Chem. Chem. Phys.* **2011**, *13*, 9789 – 9795.
[26] T. Carell, *Nature* **2011**, *469*, 45 – 46.
[27] M. Hammarson, J. Andersson, S. Li, P. Lincoln, J. Andréasson, *Chem. Commun.* **2010**, *46*, 7130 – 7132.
[28] M. J. Jorgenson, D. R. Hartter, *J. Am. Chem. Soc.* **1963**, *85*, 878 – 883.
[29] K. A. Hirose, *J. Inclusion Phenom. Macrocyclic Chem.* **2001**, *39*, 193 – 209.
[30] S. Nigam, G. Durocher, *J. Phys. Chem.* **1996**, *100*, 7135 – 7142.
[31] H. J. Hwang, S. Lee, J. W. Park, *Bull. Korean Chem. Soc.* **2000**, *21*, 245 – 250.
[32] F. B. T. Pessine, A. Calderini, G. L. Alexandrino in Review: *Cyclodextrin Inclusion Complexes Probed by NMR techniques, in: Magnetic Resonance Spectroscopy* (Ed.: D. Kim), InTechOpen, Rijeka, **2012**.
[33] R. A. Freidel, M. Orchin, *Ultraviolet Spectra of Aromatic Compounds*, Wiley, New York, **1951**.
[34] A. S. Klymchenko, V. V. Shvadchak, D. A. Yushchenko, N. Jain, Y. Mely, *J. Phys. Chem. B* **2008**, *112*, 12050 – 12055.
[35] A. K. Williams, S. C. Dasilva, A. Bhatta, B. Rawal, M. Liu, E. A. Korobkova, *Anal. Biochem.* **2012**, *422*, 66 – 73.
[36] C. Sowrirajan, S. Yousuf, I. V. M. V. Enoch, *Aust. J. Chem.* **2014**, *67*, 256 – 265.
[37] J. R. Lakowicz, *Principles of Fluorescence Spectroscopy*, Plenum Press, New York, **1999**.
[38] Y. Lu, G.-K. Wang, J. Lv, G.-S. Zhang, Q.-F. Liu, *J. Fluoresc.* **2011**, *21*, 409 – 414.
[39] a) S. J. Reshkin, R. A. Cardone, S. Harguindey, *Recent Pat. Anti-Cancer Drug Discovery* **2015**, *8*, 85 – 99; b) S. Chandrasekaran, Y. Sameena, I. V. M. V. Enoch, *J. Mol. Recognit.* **2014**, *27*, 640 – 652.
[40] A. Taenaka, E. C. M. Juan, S. Shimizu, T. Haraguchi, M. Xiao, T. Kurose, A. Ohkubo, M. Sekine, T. Shibata, C. L. Millington. RCSB Protein Data Bank Entry No. 3GJH: http://www.rcsb.org/pdb/explore/explore.do?structureId=3GJH.

Received: February 3, 2015
Published online on May 20, 2015

